A&A 376, 907–916 (2001)
DOI: 10.1051/0004-6361:20010962

Astronomy & Astrophysics

Sub-arcsec resolution near-infrared images of the Cederblad 110 region⋆

P. Persi[1], A. R. Marenzi[1], M. Gómez[2], and G. Olofsson[3]

[1] Istituto Astrofisica Spaziale, CNR, Area di Ricerca Tor Vergata, Via del Fosso del Cavaliere, 00133 Roma, Italy
[2] Observatorio Astrónomico de Córdoba, Laprida 854, 5000 Córdoba, Argentina
[3] Stockolm Observatory, 133 36 Saltsjöbaden, Sweden

Received 14 March 2001 / Accepted 4 July 2001

Abstract. We present the results of deep (K_s = 18.9) sub-arcsec resolution (0.3″) imaging observations of the Cederblad 110 region in the Chamaeleon I dark cloud. This region (roughly 5′ × 5′) is characterized by the presence of six ISOCAM-detected young stellar objects (YSOs). Our images have recovered all these sources at near-infrared (near-IR) wavelengths. Ced 110 IRS4, the brightest object in the region, is associated with a remarkable near-IR bipolar nebulosity. Ced 110 IRS6 is resolved in a double system IRS6a and IRS6b with a separation of ∼2″(∼320 AU at the distance of the Cha I cloud). We have combined 1.3 mm, far and mid-IR fluxes from the literature with our JHK data and obtained the spectral energy distributions (SEDs) for three (IRS4, IRS6a and ISO-ChaI86) of the six ISOCAM sources in the region. We modelled the SEDs of IRS6a and ISO-ChaI86 with a spherically symmetric dusty envelope, using the DUSTY code. These objects are clear Class I sources of the cloud. Finally, we report the detection of three new objects in this region (NIR 72, 84 and 89) with significant near-IR excess. If these sources are associated with the cloud, the derived luminosities and masses suggest that they are candidate young brown dwarfs of Chamaeleon I.

Key words. stars: formation – stars: low-mass, brown dwarfs – stars: pre-main sequence – infrared: stars

1. Introduction

The central part of the nearby dark cloud Chamaeleon I (D = 160 pc, Whittet et al. 1997) is characterized by the presence of the optical reflection nebula Cederblad 110 and is considered one of the most active sites of low-mass star formation of the whole dark cloud (cf. Lehtinen et al. 2001). In recent years this region has been the object of a variety of observations at different wavelengths.

Mattila et al. (1989) found a dense molecular core at the edge of the reflection nebula. Prusti et al. (1991) reported the detection of three embedded IRAS sources (Ced 110 IRS2, IRS4, and IRS6) in an area of ∼4□′ in the direction of the molecular core. Combining the IRAS fluxes with their near-infrared photometry these authors classified IRS4 and IRS6 as embedded Class I members of the cloud with luminosities of 1.4 and 1 $L_\odot$, respectively. X-ray observations of the region reported the source IRS2, coincident with the star illuminating the nebula, as one of the brightest X-ray source of the Chamaeleon I cloud (Feigelson & Kriss 1989) and more recently even IRS6, one of the lowest luminosity Class I source, was detected with $L_X \sim 10^{29-30}$ ergs s^{-1} (Carkner et al. 1998).

Millimeter continuum emission from these sources has been searched by Henning et al. (1993). Only IRS4 was detected at 1.3 mm. A subsequent continuum mapping survey at this wavelength (Reipurt et al. 1996) reported an extended object, Cha-MMS1, about 76″ south of IRS2 and IRS4 located very close to the center of a CO outflow previously found in the region by Mattila et al. (1989) and Prusti et al. (1991). Recent ISOPHOT observations between 80 and 200 μm (Lehtinen et al. 2001) classified Cha-MMS1 as a Class 0 protostar and associated this object with the probable driving source of the Herbig-Haro objects HH 49 and 50 (Schwartz 1997).

In the Ced 110 area, Persi et al. (2000) found six sources with ISOCAM at 6.75 and 14.3 μm with a clear mid-IR excess due mainly to circumstellar dust material. Three of these sources, ChaI75, ChaI84 and ChaI92, were identified with IRS2, IRS4 and IRS6, respectively. Figure 1 shows the ISOCAM image at 14.3 μm of the Ced 110 dense core with the designation of the sources. The ChaI numbers are relative to the list of sources given in Persi et al. (2000). The ISOCAM observations reinforce the

Send offprint requests to: P. Persi,
e-mail: persi@ias.rm.cnr.it

⋆ Based on observations collected at the European Southern Observatory, Chile, ESO proposal N.65.I-0054.

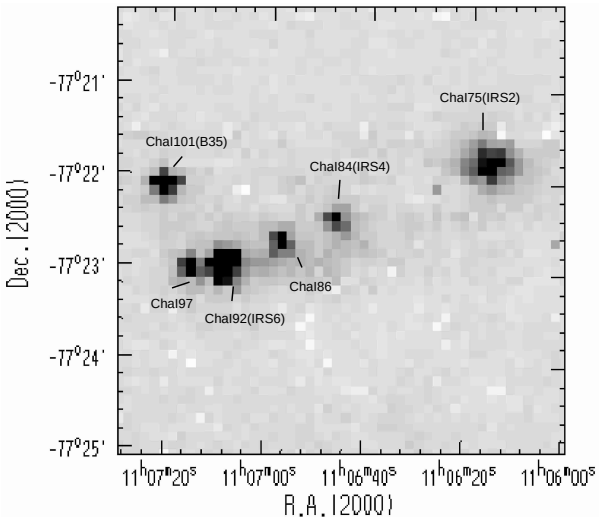

Fig. 1. ISOCAM image at 14.3 μm of the Ced 110 region.

conclusion of a high star-formation efficiency ($\sim$20%) in this region, suggested by Lehtinen et al. (2001).

Large field near-infrared (near-IR) imaging surveys of Chamaeleon I dark cloud that include the Ced 110 area, have been obtained by DENIS (Cambrésy et al. 1998) and very recently by Gómez & Kenyon (2001). The modest spatial resolution and the limited sensitivity of these two surveys do not add anything to the knowledge of the region around Ced 110. On the contrary, deep and high resolution photometric near-IR images can be fundamental in studying the circumstellar material around solar-type young stellar objects and to detect the lowest luminous young stellar population in nearby dark clouds. In fact, Persi et al. (1999) from deep near-IR images of the northern part of Chamaeleon I (ChaI North) suggest the presence of a very low luminosity young stellar population not detected by ISOCAM. J, H, and K sub-arcsec resolution images (0.147″/pixel) of Ced 110 IRS4 taken with the VLT/UT1 telescope (Zinnecker et al. 1999) indicate a complex structure around this young stellar object (YSO), with a north-south infrared reflection nebula bisected by a patchy east-west dark lane with a highly reddened central point source. No photometric study is given from these VLT high resolution images.

In this paper, we present the results of our very deep and high resolution broad-band near-IR imaging photometry of a region of about $5' \times 5'$ around the Ced 110 dense core. We detected 165 sources in K_s, 148 in H and 91 in J bands at 3σ level. We used the color-color $J-H/H-K$ diagram together with the K_s-magnitude distribution to identify new members of the cloud and selected three candidates with significant near-IR excess. We derive luminosities and visual extinction for the ISOCAM sources in the region as well as for the newly near-IR selected stars. We combine millimeter, far and mid-IR fluxes from the literature with our JHK_s photometry to obtain and to analyze the spectral energy distributions (SEDs) of three of the ISOCAM sources in the region.

2. Observations and results

We have obtained J, H, and K_s images of the Cederblad 110 region, covering an area of about $4.9' \times 4.9'$ and centered on the source IRS4. The images, corresponding to the same area as the 14.3 μm data (see Fig. 1), have been obtained with the SOFI near-IR camera at the ESO 3.58 m New Technology Telescope (NTT) on the night of 2000 April 28 under very good seeing conditions ($\sim$0.3″). The K_s filter is centered at 2.162 μm with $\Delta\lambda = 0.275$ μm. The JHK_s images are shown in Fig. 2.

SOFI has a 1024×1024 pixel HgCdTe array and provides a field of view of $299'' \times 299''$ with a scale of 0.292″/pix. The near-IR images were taken in *jitter* mode (see the ESO-SOFI manual) with 8 single frames each of 60 sec exposure time, and with a jitter width of 40″. The Deep Infrared Mosaicing Software (*Dimsum*) developed by Eisenhardt et al. as user–contributed package for IRAF[1] was used to get correctly sky subtracted images, and then the *Jitter* data reduction software developed by Devillard (1997) was applied on these images, to obtain the final co-added images given in Fig. 2.

Flux calibration was made by observing the infrared NICMOS standard star S064-F from the list of Persson et al. (1998), before and after the observations of Ced 110 region. Stellar photometry of the detected sources, was performed using the DAOPHOT (Stetson 1987) routine within IRAF with an aperture of 1.5″. The coordinates of the near-IR sources were derived comparing our images with the Digitized Sky Survey (DSS) plates. We estimate an average uncertainty of $\sim$1″ for our coordinates. The 3σ limiting magnitudes (for point-like sources) are $J = 21.4$, $H = 20.0$ and $K_s = 18.9$. At these limits we detected 165 sources at K_s, 148 at H and 91 at J. The complete list of the detected sources with their photometry and positions is available in electronic form.

3. Discussion

In our images of Fig. 2, and in particular on the K_s-band, all the ISOCAM sources in the region detected at 14.3 μm and classified as YSOs are clearly visible. IRS2 is saturated in our images. IRS4 is associated with a remarkable nebulosity. The Class I young stellar object IRS6 appears double, and halfway between IRS4 and IRS6 we detect the near-IR counterpart of the ISOCAM source ChaI86 (Persi et al. 2000) not found by DENIS, and observed at 80 μm (Ced 110 IRS11 in Lehtinen et al. 2001).

We have not detected in our near-IR images the far-IR source Ced 110 IRS10 identified by Lehtinen et al. (2001) with the millimeter source Cha-MMS1. This source was neither found by ISOCAM at a detection limit of $\sim$0.7 mJy and 1.3 mJy (1σ) at 6.75 and 14.3 μm, respectively (Persi et al. 2000). The lack of near and mid-IR

[1] IRAF is distributed by the National Optical Astronomy Observatory, which is operated by the Association of Universities for Research in Astronomy Inc. under contract to the National Science Foundation.

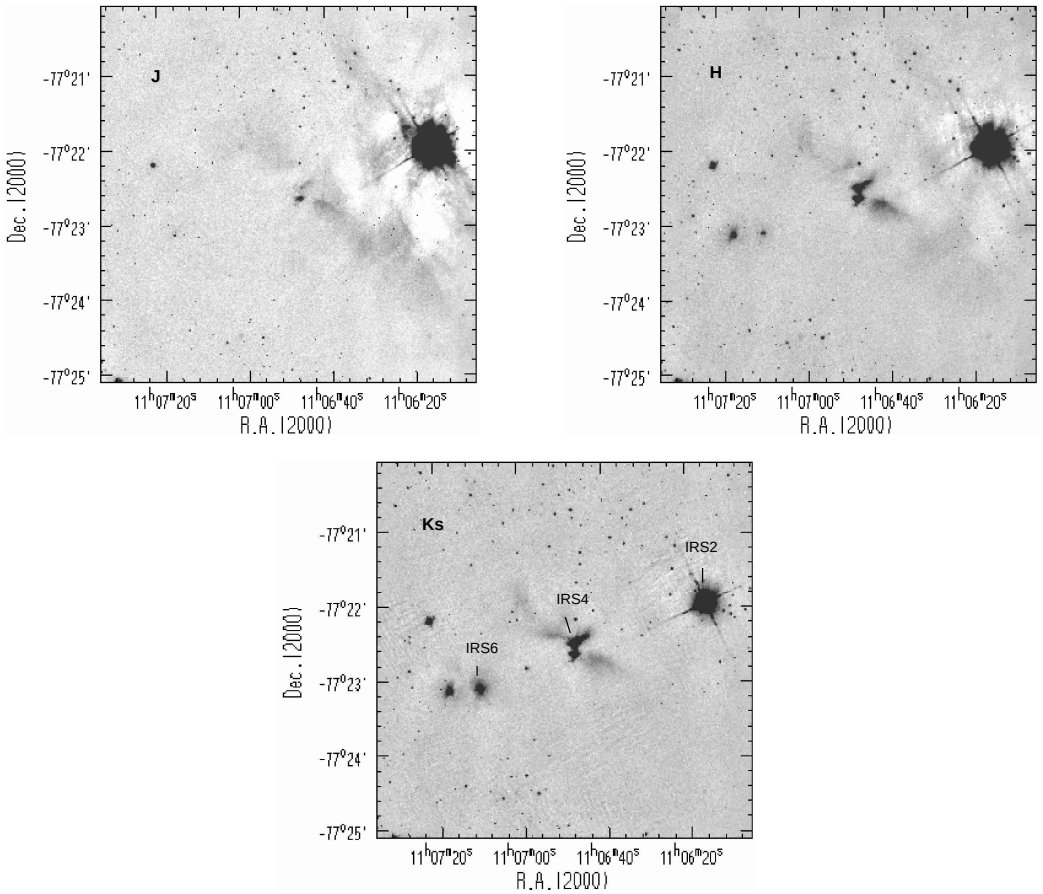

Fig. 2. JHK_s images of Ced 110 region. The positions of IRS2, IRS4 and IRS6 are marked on the K_s image.

emission in Cha-MMS1, and the shape of its energy distribution between 80 and 1300 μm (see Lehtinen et al. 2001), confirm that this source is a Class 0 protostar.

The ISOCAM sources detected in the region, with the exception of ISO-ChaI101 identify with B35 (Baud et al. 1984), appear to form a chain of YSOs aligned along the direction NW-SE of the dense molecular core (Fig. 1). This is also illustrated in Fig. 3, the true-color image obtained combining the J image in blue, the H image in green, and the K_s in red. From this combined image we have excluded the saturated source IRS2. Figure 3 is very similar in sensitivity and spatial resolution to the images obtained with the VLT by Zinnecker et al. (1999). IRS6 is resolved in two very red objects (IRS6a and IRS6b) separated by $\sim 2''$ (320 AU) in the E-W direction. IRS4 is associated with north-south bipolar reflection nebula, with a highly reddened central point source. We will return to these sources in the next subsection and compare our near-IR observations with published data at longer wavelengths.

3.1. Near-infrared colors

Using the near-IR sources detected in all the three filters, we have derived the $J-H/H-K$ color-color diagram of Fig. 4. The loci of intrinsic colors for dwarfs and giant stars (Bessel & Brett 1988) are indicated with the solid line in Fig. 4, while the dashed lines define the reddening band extending from dwarfs and giants stars ($E(J-H)/E(H-K) = 1.80$; Gómez & Kenyon 2001). The colors of un-reddened classical TTauri stars (CTTSs, Meyer et al. 1997) are also shown. Most of the observed sources lie along the reddening band and do not show significant near-IR excess. These sources include reddened background stars as well as likely weak emission T Tauri stars (WTTs, class III sources) members of the cloud. The WTTs, as a class of YSOs, do not have significant near-IR excess. In addition, four of the ISOCAM sources in the region, classified as YSOs from mid-IR color excess (Persi et al. 2000), lie within the reddening band. Therefore the near-IR color-color diagram does not always allow one to assert the nature of sources without near-IR color excess.

Two sources in Fig. 4 (NIR72 and NIR84) with good photometric accuracy have clear near-IR excess, consistent with those of reddened CTTs. These sources are candidate Class II members of the cloud. NIR89, on the contrary, cannot be de-reddened to the CTTs line and thus is a potential Class I source of the cloud.

We believe that these sources, not detected by ISOCAM, are new members of the dark cloud. As shown below, the obscuration towards this region is high ($A_V = 14$) and we expect that there is a small risk of contamination by background galaxies. At this Galactic latitude, the probability of finding an evolved star with near-IR

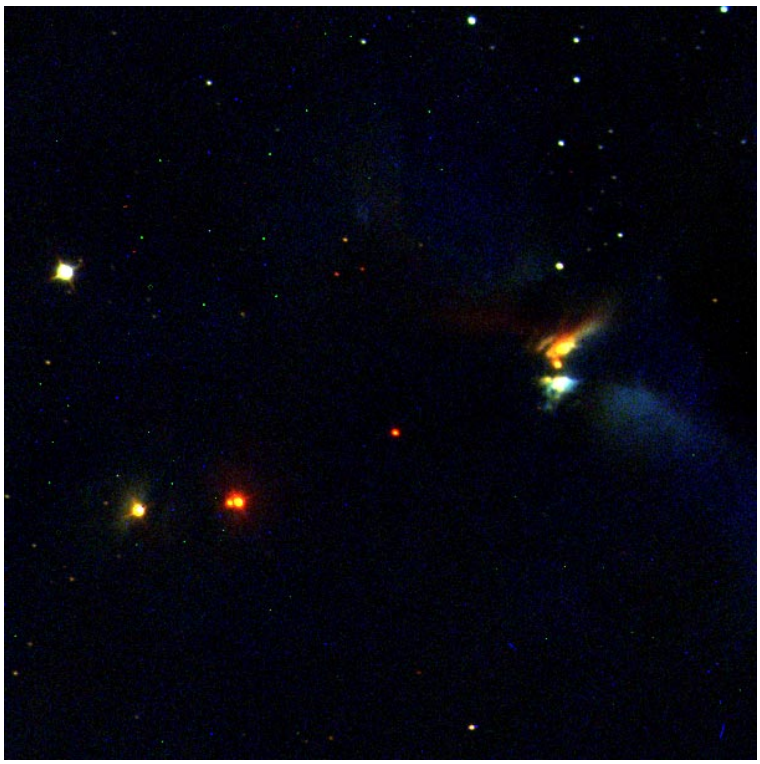

Fig. 3. *True color* image of Ced 110 obtained from J (blue), H (green) and K_s (red) individual images. The size of the image is $3'.\!\!' \times 3'.\!\!'$.

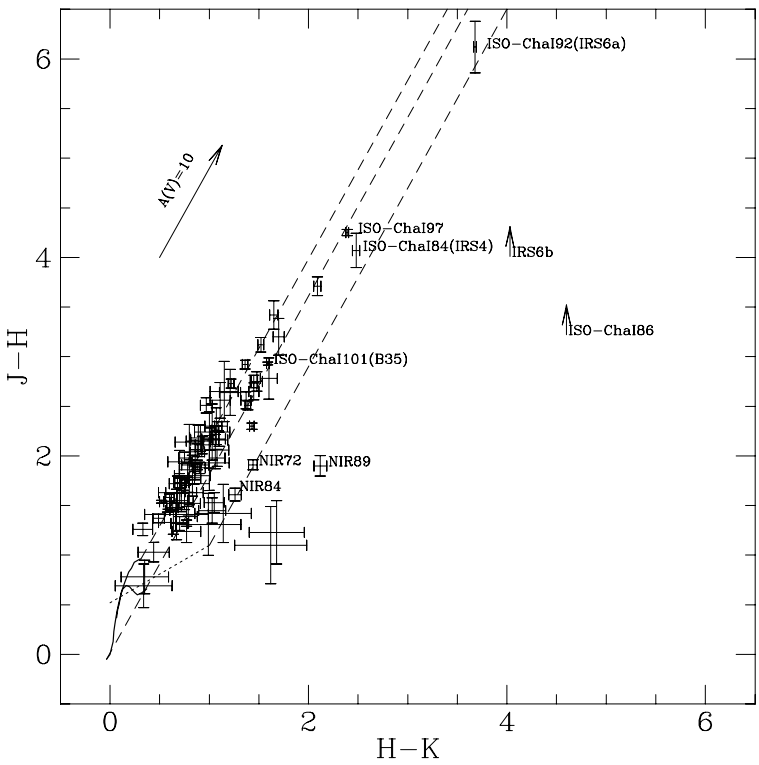

Fig. 4. J–H vs. H–K diagram of 91 sources detected in Ced 110. The location of the ISO sources and of three new candidates YSOs are shown. The solid line indicate the main sequence locus (Bessel & Brett 1988). The dashed lines define the reddening band extending from the main sequence and using the reddening vector $E(J-H)/E(H-K) = 1.80$ (Gómez & Kenyon 2001). The dotted line represent the colors of un-reddened CTTSs (Meyer et al. 1997).

Table 1. Positions and photometry of the ISOCAM and the new sources with near-IR excess.

Source	α(2000)	δ(2000)	J	H	K_s	ID.
	h m s	° ′ ″	mag	mag	mag	
NIR72	11 06 46.8	−77 22 37	18.07	16.16	14.72	
NIR76	11 06 47.1	−77 22 34	20.53(.17)	16.46	13.98	ISO-ChaI84(IRS4)
NIR84	11 06 51.1	−77 20 07	19.16(.05)	17.55	16.29(.05)	
NIR89	11 06 53.8	−77 24 00	19.60(.09)	17.70(.05)	15.58	
NIR98	11 06 58.8	−77 22 50		18.18(.07)	13.58	ISO-ChaI86
NIR118	11 07 09.9	−77 23 06	20.99(.26)	14.88	11.19	ISO-ChaI92(IRS6a)
NIR120	11 07 10.5	−77 23 06		17.39	13.36	ISO-ChaI92(IRS6b)
NIR131	11 07 17.0	−77 23 08	18.13	13.88	11.49	ISO-ChaI97
NIR141	11 07 21.7	−77 22 12	15.36	12.43	10.84	ISO-ChaI101(B35)

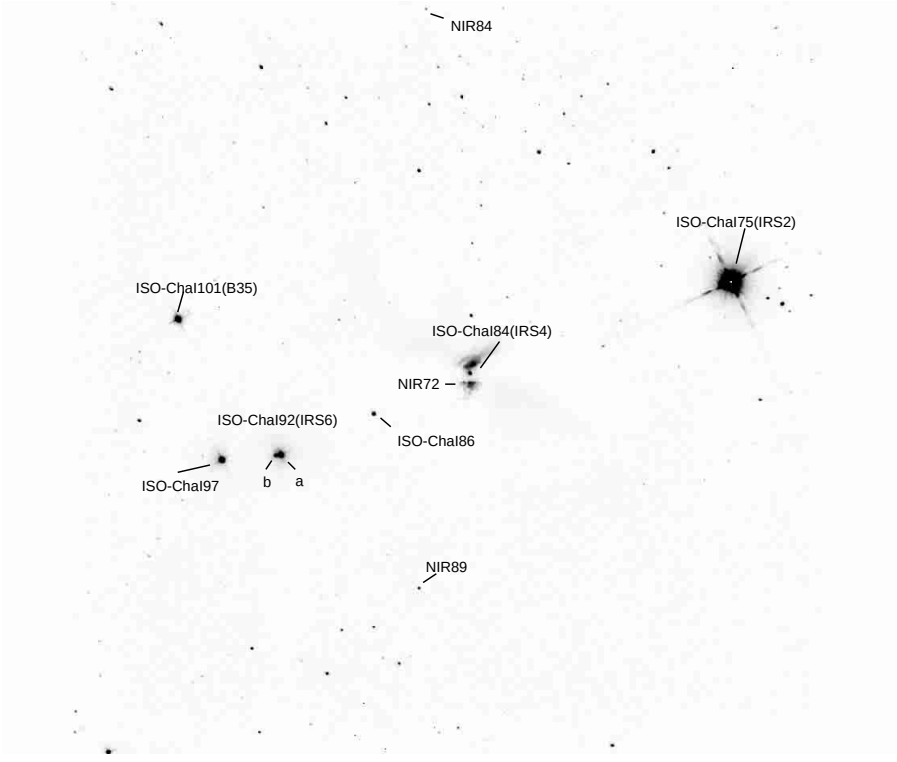

Fig. 5. K_s image of Ced 110. The ISOCAM sources in the region as well as the new near-IR candidate YSOs are labelled. North is at the top and East to the left. The size of the image is $4.9' \times 4.9'$.

excess emission is low within such a small field (cf. Gómez & Kenyon 2001). In Table 1 we report the photometry and the positions of the three new sources with near-IR excess (NIR72, NIR84, and NIR89), as well as previously known ISOCAM sources in the region. The designation of the sources is the same as in the general list published in electronic form. The statistical errors are reported in brackets. Where not indicated, the errors are less than ± 0.05 mag. These objects are labelled over the K_s image of Fig. 5.

The source NIR72 is located approximately $2.8''$ east of the southern lobe of the source IRS4. It may form part of the IRS4 complex as suggested by the H and K_s contour maps in Fig. 6. On the contrary, NIR84 and NIR89 appear isolated on the K_s image. The three sources are not visible on the DSS plates.

We used the 91 sources detected in the three bands to estimate extinction towards the Ced 110 region. We previously eliminated known YSOs and new detections showing near-IR excess. In this manner we obtained a sub-sample of 73 sources. Although this sub-group may include young stars with no near-IR excess, their spatial distribution is fairly random and shows no correlation with the positions of known young objects in the region. This sub-sample should correspond to the stellar population behind the cloud and will be used to derive the extinction towards this region. These 73 stars have average colors $(H-K)$ and $(J-H)$ of 0.83 ± 0.04 and 1.93 ± 0.06, respectively. Gómez & Kenyon (2001) obtained JHK data for three

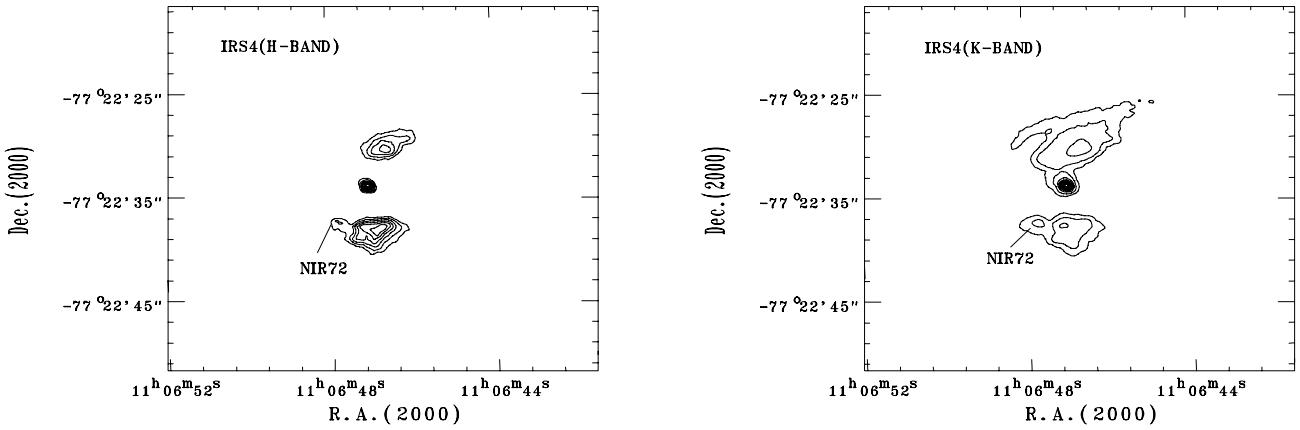

Fig. 6. H and K_s-contour maps of the source IRS4. The position of the source NIR72 is indicated.

off-cloud regions. These control fields or un-reddened areas are located relatively close to the Ced 110 and can be used to estimate the average colors of background stars assuming that the stellar population behind the Ced 110 region is identical to stellar population in these control fields. Background stars in Gómez & Kenyon's off-cloud regions have $(H-K)$ and $(J-H)$ of 0.09 ± 0.01 and 0.43 ± 0.04, roughly corresponding to a G8–K2 main sequence star (Koornneef 1983; Bessell & Brett 1988). Due to the galactic position of the Ced 110 region, away from the plane ($b \sim -15.7°$), it is natural to expect that an average background star in this area would be a late type star. Early spectral types (O, B, and A) tend to concentrate towards the galactic plane.

We compared the average colors of stars in the Ced 110 region with those of a "typical" G8–K2 background star. The corresponding color excess for sources in the observed region are: $E(H-K) = 0.74 \pm 0.04$ and $E(J-H) = 1.50 \pm 0.07$. Using Rieke & Lebofsky (1985) standard reddening law we derive $A_K = 1.78\,E(H-K)$ and $A_K = 1.05\,E(J-H)$. We applied these relations finally adopt an average $A_K = 1.4$ mag. On average, the stars in the Ced 110 region are affected by $A_V = 14$ mag.

The extinction law $E(J-H)/E(H-K) = 2.03 \pm 0.09$ derived for the Ced 110 region and that obtained by Gómez & Kenyon (2001) for the whole Chamaeleon I dark cloud using a different K-band filter, $E(J-H)/E(H-K) = 1.80 \pm 0.03$, differ at roughly the 2σ level. This difference may provide support for earlier results indicating a variation of the extinction across the Cha I dark cloud (see, for example, Whittet et al. 1997; Hayakawa et al. 1999). However, we notice that a more precise and careful determination of the extinction towards the Ced 110 region that includes the measurement of a corresponding control field is required before claiming such variation.

3.2. K-magnitude distribution

Figure 7 shows the K_s-magnitude histogram for the 165 K_s sources with a signal-to-noise ratio of $\geq$3 and corrected for an average $A_K = 1.4$ mag. The dashed line reproduces the expected distribution of field stars in an identical area and at the same galactic coordinates as the Ced 110 region, computed from the Besançon model (Bienaymé et al. 1987). The model reproduces fairly well the distribution of our de-reddened sources up to the completeness limit of our observations, $m_0(K_s) = 16.5$. This result suggests that most of the sources in the Ced 110 region are reddened field stars.

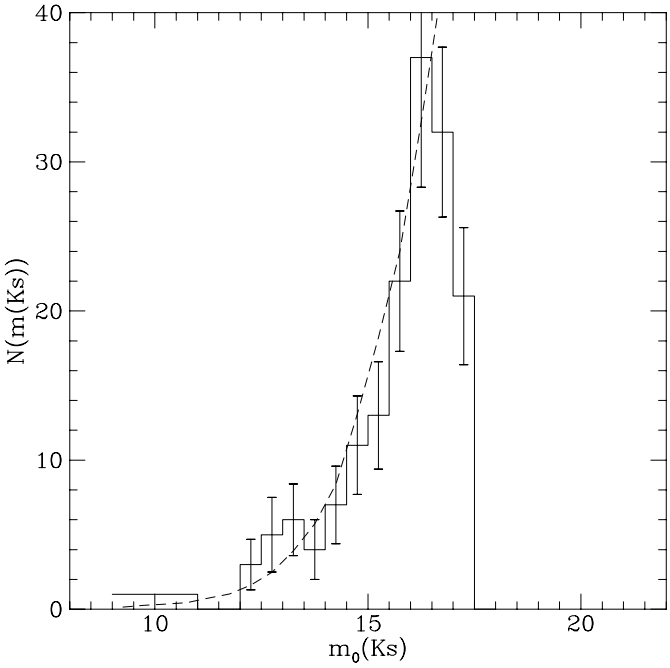

Fig. 7. K-magnitude distribution histogram for all sources detected in the K_s image of Ced 110 corrected for $A_K = 1.4$. The error bars correspond to the statistical errors for each bin. The dashed line represents the number of stars predicted by the Becançon model in an identical area and the same galactic position as the Ced 110 region.

3.3. Stellar luminosities

We have estimated the stellar luminosities for the sources of Table 1 using the de-reddened J-band fluxes. This method, appropriate for Class I, and Class II (CTT)

stars, is described in detail by Persi et al. (2000) and Bontemps et al. (2001). Basically, we have converted the absolute J-band magnitude, M_J, in the stellar luminosity $L\star$ using the following relation:

$$\log L(L_\odot) = 1.89 - 0.4(J - DM - A_J + BC_J(T_{\rm eff}))$$

where J is the measured J-band magnitude, $DM = 6.02$ is the distance modulus, and $A_J = 2.63[(J-H)-(J-H)_0]$. This last relation has been obtained using the Rieke & Lebofsky (1985) reddening law. We have adopted for all the sources the mean intrinsic color for un-reddened CTTs of $(J-H)_0 = 0.85$ (Meyer et al. 1997). This is justified by the fact that the dispersion in intrinsic $(J-H)$ colors of CTTs is small and observationally well determined. The bolometric correction for the J band depends only on $T_{\rm eff}$. Considering that pre-main sequence stars have photospheric temperatures in the range 2500–5500 K, the BC_J correction spans only a limited range (1–2). Therefore, by adopting in our estimations an average $T_{\rm eff} = 3700$ K corresponding to $BC_J = 1.65$ (Kenyon & Hartmann 1995), we introduce an uncertainty not larger than $\pm 0.1-0.2$ dex in $\log(L\star)$. Combining different sources of uncertainties (such as photometric, intrinsic colors, BC_J corrections, and distance errors) we estimate a total uncertainty in $L\star$ of $\sigma(\log L\star) \sim 0.2-0.3$ dex. Finally, for three sources with a good spectral coverage (ChaI92(IRS6a), ChaI97, and ChaI101), we have obtained the infrared luminosity integrating the de-reddened spectral points. The derived infrared luminosities appears a factor $\sim$2 higher than those obtained from the de-reddened J photometry.

Table 2 gives A_V, M_J, $L\star$ and two values of masses for each source of Table 1. The luminosity derived for IRS4 is relative only to the central reddened star. This can explain the disagreement with the bolometric luminosity estimated by Prusti et al. (1991). The values of masses were derived assuming ages of 1 Myr and 10 Myr, respectively, and using the D'Antona & Mazzitelli (1998) $M\star$ – $L\star$ relation for very low mass stars. From the above evaluation of the error in the luminosity, we estimate an accuracy of a factor of 2 in the derived masses.

Assuming that the three new sources with near-IR excess (NIR72, NIR84 and NIR 89) are members of the cloud and even considering the uncertainty in $L\star$ and age we find that these objects have masses well below the brown dwarf limit (0.08 $M_\odot$). These sources are thus good new candidate young brown dwarfs of the cloud. The presence of other young sub-stellar members in the Cha I dark cloud have recently been shown by Neuhäuser & Comerón (1999), Oasa et al. (1999), and Persi et al. (2000).

3.4. Spectral energy distribution

We have obtained the spectral energy distributions (SEDs) for three ISOCAM sources in the Ced 110 region (ChaI84, ChaI92, and ChaI96), combining our near-IR observations and the published flux densities at mid, far-IR and millimeter wavelengths. In addition we include the circular variable filter (CVF) observations taken with ISOCAM, and obtained from the ISO Data Center (program 71801902). These data are normalized to fit the broad-band mid-IR fluxes. IRAS flux densities corresponding to these sources have been excluded from our analysis. Sources confusion problems make these fluxes rather uncertain. Lehtinen et al. (2001) have also presented a discussion the SEDs of these three sources based on their measured far-IR fluxes.

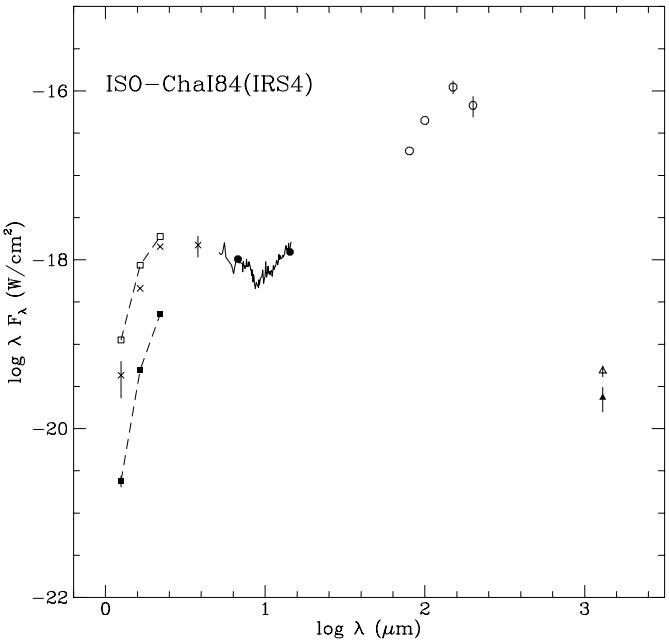

Fig. 8. The spectral energy distribution of IRS4. Filled squares correspond to our near-IR data for an aperture of 1.5″and open squares to an aperture of 12″. Prusti et al. (1991) near-IR data are represented by crosses. Mid-IR fluxes (filled circles) and far-IR (open circles) were obtained from Persi et al. (2000) and Lehtinen et al. (2001). Continuum millimeter data at 1.3 mm are plotted as open and filled triangles, Henning et al. (1993) and Reipurth et al. (1993), respectively. The thick line shows the ISOCAM CVF observations.

3.4.1. ISO-ChaI84(IRS4)

As well illustrated in Fig. 3, IRS4 exhibits a complex structure with the presence of a very red central source and a bipolar reflection nebula extending north-south with a size of approximately $20 \times 25\square''$. The north lobe is redder than the south, probably indicating the effect of differential extinction. In addition a fainter, and more extended infrared nebulosity is observed south-west and north-east of IRS4 (see Fig. 2). This morphological complexity makes a comparison among observations at different wavelengths very difficult given the different apertures used. In any event we show in Fig. 8 the SED of IRS4 including our near-IR flux densities computed for an aperture of 1.5″ (central star) and 12″, the same used by Prusti et al. (1991) in their near-IR photometry. The far-IR and millimeter continuum observations indicate the presence of a very cold dust in IRS4 ($T_{\rm d} = 21$ K, Lehtinen et al. 2001) while

Table 2. Physical parameters of the ISOCAM and the new sources with near-IR excess.

Source	A_V	M_J	$L_\star(L_\odot)$	1 MYr($M_\odot$)	10 MYr($M_\odot$)
NIR72	9.9	9.3	3.4×10^{-3}	0.020	0.035
ISO-ChaI84(IRS4)	30.0	6.1	6.5×10^{-2}	0.10	0.32
NIR84	7.1	11.1	6.0×10^{-4}	0.015	0.020
NIR89	9.8	10.8	8.0×10^{-4}	0.016	0.021
ISO-ChaI92(IRS6a)	49.1	1.1	6.0	1.99	1.60
ISO-ChaI97	31.8	3.2	0.9	0.56	1.10
ISO-ChaI101	19.4	3.9	0.5	0.40	1.00

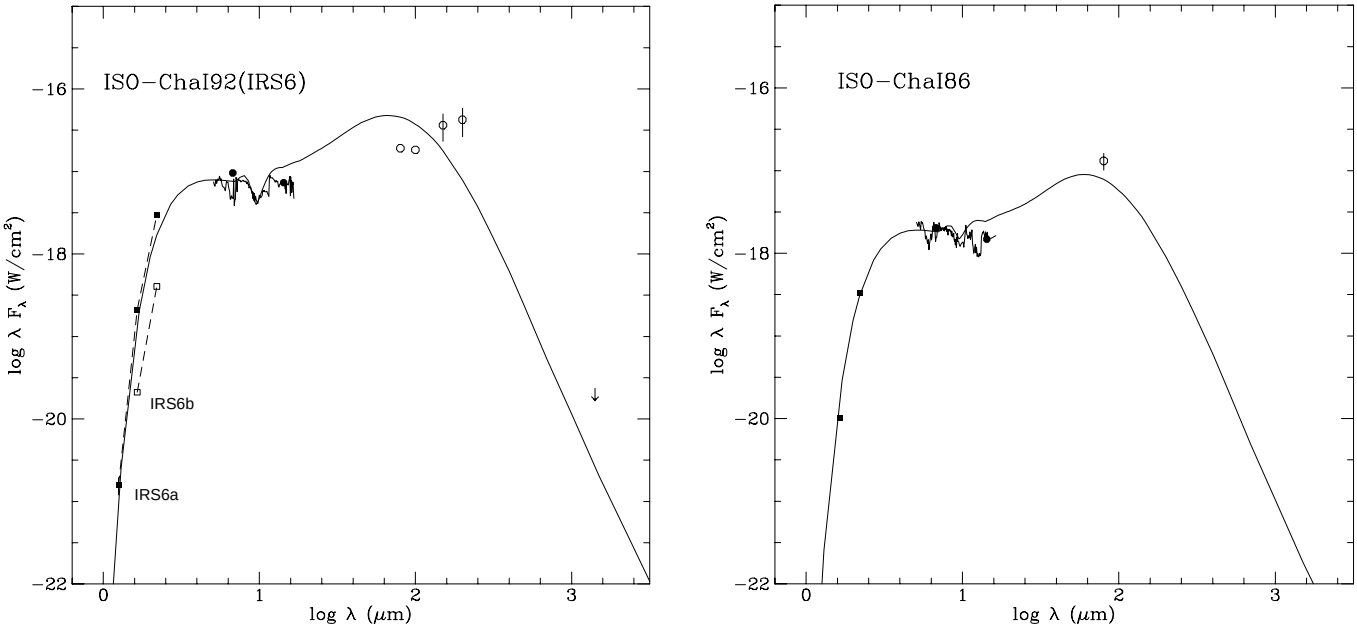

Fig. 9. SEDs of the sources ISO-ChaI92(IRS6), left panel, and ISO-ChaI86, right panel. Symbols as in Fig. 8. The continuous line indicates the spherically symmetric dusty model from the DUSTY code. The parameters of the model are given in Table 3.

the ISOCAM CVF data (thick line in Fig. 8) show the presence of the silicate absorption band at 9.8 μm.

3.4.2. ISO-ChaI92(IRS6) and ISO-ChaI86

The SEDs of the double system IRS6 and of the new YSO discovered by ISOCAM, ISO-ChaI86, are shown in Fig. 9. The brightest component of the double system, IRS6a (Fig. 5), has a near-IR luminosity about a factor of 7 higher than IRS6b and similar $H-K$ color. This suggests that most of the flux density observed in the mid-IR by ISOCAM ($ap = 6''$) and far-IR by ISOPHOT (Lehtinen et al. 2001) is associated with IRS6a. We have used the DUSTY code (Ivezić et al. 1999), developed for spherically symmetric dust envelopes (Ivezić & Elitzur 1997), to compare the observed spectral points of IRS6a and ISO-ChaI86 with a synthetical model produced by this code. As input of the model we have fixed the temperature of the central source, $T_e = 4000$ K, the temperature at the inner radius ($T_1 = 1300$ K), and an adopted density distribution of the type $n(r) \propto r^{-0.5}$.

The weak silicate absorption bands at 9.8 μm observed by ISOCAM put a constraint on the nature and optical properties of the dust grains. We have adopted a mixture of silicates and graphite grains using the optical constants of Draine & Lee (1984), and a grain size distribution $n(a) \propto a^{-3.7}$ with a in the range 0.01 to 0.24 μm. The DUSTY models are represented by continuous lines in Fig. 9 and the derived parameters for the two sources, such as optical depth τ_V, inner (r_i) and outer (r_o) radii, and temperature of the dust T_d at r_o, are given in Table 3. The bolometric luminosity of IRS6a computed from the model is roughly a factor 1.7 higher than deduced from the de-reddened J-photometry (see Table 1). This result confirms the validity of the method described in Sect. 3.3 to derive the stellar luminosity.

We notice that for both sources, the DUSTY code fits fairly well the SEDs from the near to the mid-IR wavelengths. On the other hand, in the far-IR spectral range the fitting is rather poor, with an average discrepancy of about 0.3 in $\log \lambda F_\lambda$. IRS6 and ISO-ChaI86, as well as IRS4, are not well resolved in the far-IR spectral range (see contour maps at 100, 150, and 200 μm of

Table 3. Model parameters derived from the DUSTY code.

Source	τ_V	r_i (cm)	r_o (cm)	T_d (K)	L_{Bol} $L_\odot$	α_{IR}
IRS6a	70	1.8×10^{12}	9.0×10^{15}	21	10	0.5
ISO-ChaI86	70	7.8×10^{11}	2.3×10^{15}	25	0.17	0.8

Lehtinen et al. 2001). Contamination from nearby sources may affect the flux determinations at long wavelengths and thus explain at least part of the difference between the DUSTY model and the observed points.

We have computed the infrared spectral index $\alpha_{IR} = \mathrm{d}\log\lambda F_\lambda / \mathrm{d}\log\lambda$ from 2.2 μm and 14.3 μm for these two sources. The values of $\alpha_{IR} = 0.5$ and 0.8 have been obtained for IRS6a and ISO-ChaI86, respectively, indicating that these sources are Class I YSOs. Finally, the parameters derived from the DUSTY model show that IRS6a and ISO-ChaI86 are very similar to each other, having very cold dust and being deeply embedded in the cloud material. It is interesting to note that Class I sources in the cloud are rare (Persi et al. 2000). One of the few previously known Class I sources was found by Persi et al. (1999) in the ChaI North associated with a bipolar outflow.

4. Conclusions

We have imaged at sub-arcsec resolution and high sensitivity in the near-IR the central part of the Ced 110 reflection nebula in the Chamaeleon I dark cloud. This region includes six ISOCAM sources. From the analysis of these images we obtain the following conclusions:

1) We detected a total of 165 point sources in the K_s band in the $4.9' \times 4.9'$ field around the Ced 110 reflection nebula. Only 91 of the sources (i.e. 55%) are also detected at both J and H bands. The color-color $J-H/H-K$ diagram shows that most of the sources have no significant near-IR excess (see Fig. 4). This is also true for four of the ISOCAM sources in the region previously classified as YSOs from mid-IR observations. As consequence near-IR observations can not always discriminate YSOs from reddened background stars.

2) Comparing the un-reddened K_s-magnitude distribution of all sources detected in the Ced 110 with the number of field stars expected in an identical area at the same galactic position we conclude that most of the observed sources are likely reddened background stars in agreement with our color-color diagram discussion.

3) Three new sources, NIR72, 84 and 89, show clear near-IR excess. If the sources are members of the cloud, their derived stellar luminosities from the near-IR observations, indicate these sources as good candidate young brown dwarfs of the cloud. NIR72 and 84 show color excess compatible with that of Class II objects, while NIR89 is a potential Class I source of the cloud. Further images in the L and M bands at similar spatial resolution as present data, are necessary to confirm whether NIR72 is a real point like YSO or whether it forms part of the complex nebulosity surrounding IRS4.

4) Our sub-arcsec near-infrared images show a complex morphology for the source IRS4 (Fig. 3), with a very red central star surrounded by a bipolar reflection nebula extending north-south. In addition, we identify a double system of YSOs (IRS6a and IRS6b) associated with the source IRS6.

5) From the analysis of the SEDs of IRS6a and ISO-ChaI86, we classify these two sources as Class I YSOs. Apart from the different luminosities, the sources show very similar properties as derived from the fit of their SEDs with a spherically symmetric dust envelope model (see Fig. 9).

Finally, the presence of these two confirmed Class I sources, as well as the Class I candidate (NIR89), and the millimeter source Cha-MMS1 identified by Lehtinen et al. (2001) as a Class 0 protostars, suggest that the Ced 110 area is probably the youngest and the most active site of low mass star formation within the Chamaeleon I cloud.

Acknowledgements. We are grateful to the ESO staff for assistance during the observing run, specially to Leonardo Vanzi for technical support with SOFI. We also thank Timo Prusti, the referee, for helpful comments and suggestions which improved the paper.

References

Baud, B., Young, E., Beichman, C. A., et al. 1984, ApJ, 278, L53
Bessel, M. S., & Brett, J. M. 1988, PASP, 100, 1134
Bienaymé, O., Robin, A. C., & Creze, M. 1987, A&A, 180, 94
Bontemps, S., André, P., Kaas, A. A., et al. 2001, A&A, 372, 173
Cambrésy, L., Copet, E., Epchtein, N., et al. 1998, A&A, 338, 977
Carkner, L., Kozak, J. A., & Feigelson, E. D. 1998, AJ, 116, 1933
D'Antona, F., & Mazzitelli, I. 1998, in Brown Dwarfs and Extrasolar Planets, ed. R. Rebolo, E. L. Martin, & M. R. Zapaterio Osorio, ASP Conf. Ser., 134, 442
Devillard, N. 1997, The Eclipse Software, The Messanger, 87
Draine, B. T., & Lee, H. M. 1984, ApJ, 285, 89
Feigelson, E. D., & Kriss, G. A. 1989, ApJ, 338, 262
Gómez, M., & Kenyon, S. J. 2001, AJ, 121, 974
Hayakawa, T., Mizuno, A., Onishi, T., et al. 1999, PASP, 51, 919
Henning, Th., Pfau, W., Zinnecket, H., & Prusti, T. 1993, A&A, 276, 129
Kenyon, S. J., & Hartmann, L. 1995, ApJS, 101, 117

Koornneef, J. 1983, A&A, 128, 84
Ivezić, Z., & Elitzur, M. 1997, MNRAS, 287, 799
Ivezić, Z., Nenkova, M., & Elitzur, M. 1999, User Manual for DUSTY (University of Kentucky), Internal Report, available at `http:www.pa.uky.edu/moshe/dusty`
Lehtinen, K., Haikala, L. K., Mattila, K., & Lemke, D. 2001, A&A, 367, 311
Mattila, K., Liljeström, T., & Toriseva, M. 1989, in Low Mass Star Formation and Pre-Main Sequence Objects, ed. B. Reipurth, ESO Conf. Proc., 33, 153
Meyer, M. R., Calvet, N., & Hillebrand, L. A. 1997, AJ, 114, 288
Neuhäuser, R., & Comerón, F. 1999, A&A, 350, 612
Oasa, Y., Tamura, M., & Sugitani, K. 1999, ApJ, 526, 336
Persi, P., Marenzi, A. R., Kaas, A. A., et al. 1999, AJ, 117, 439
Persi, P., Marenzi, A. R., Olofsson, G., et al. 2000, A&A, 357, 219
Persson, S. E., Murphy, D. C., Kreminski, W., et al. 1998, AJ, 116, 2475
Prusti, T., Clark, F. O., Whittet, D. C. B., et al. 1991, MNRAS, 251, 303
Reipurth, B., Chini, R., Krügel, E., et al. 1993, A&A, 273, 221
Reipurth, B., Nyman, L.-A., & Chini, R. 1996, A&A, 314, 258
Rieke, G. K., & Lebofsky, M. J. 1985, ApJ, 288, 618
Schwartz, R. D. 1977, ApJS, 35, 161
Stetson, P. B. 1987, PASP, 99, 101
Whittet, D. C. B., Prusti, T., Franco, G. A. P., et al. 1997, A&A, 327, 1194
Zinnecker, H., Krabbe, A., McCaughrean, M. J., et al. 1999, A&A, 352, L73